Network analysis of differential Ras isoform mutation effects on intestinal epithelial responses to TNF-#

Citation: Lau, Ken S., Sarah B. Schrier, Jessica Gierut, Jesse Lyons, Douglas A. Lauffenburger, and Kevin M. Haigis. "Network Analysis of Differential Ras Isoform Mutation Effects on Intestinal Epithelial Responses to TNF-α." Integrative Biology 5, no. 11 (2013): 1355.

As Published: http://dx.doi.org/10.1039/c3ib40062j

Publisher: Royal Society of Chemistry

Persistent URL: http://hdl.handle.net/1721.1/99482

Version: Author's final manuscript: final author's manuscript post peer review, without publisher's formatting or copy editing

Published in final edited form as:
Integr Biol (Camb). 2013 November ; 5(11): 1355–1365. doi:10.1039/c3ib40062j.

Network Analysis of Differential Ras Isoform Mutation Effects on Intestinal Epithelial Responses to TNF-α†

Ken S. Lau[a,b,‡], **Sarah Schrier**[b,‡], **Jessica Gierut**[a], **Jesse Lyons**[a,b], **Douglas A. Lauffenburger**[b,*], and **Kevin M. Haigis**[a,*]

[a]Molecular Pathology Unit, Center for Cancer Research, and Center for Systems Biology, Massachusetts General Hospital, 149 13th Street, Charlestown, MA 02129

[b]Department of Biological Engineering, Massachusetts Institute of Technology, 77 Massachusetts Avenue, Cambridge, MA 02139

Abstract

Tumor necrosis factor alpha (TNF-α) is an inflammatory cytokine that can elicit distinct cellular behaviors under different molecular contexts. Mitogen activated protein kinase (MAPK) pathways, especially the extracellular signal-regulated kinase (Erk) pathway, help to integrate influences from the environmental context, and therefore modulate the phenotypic effect of TNF-α exposure. To test how variations in flux through the Erk pathway modulate TNF-α-elicited phenotypes in a complex physiological environment, we exposed mice with different Ras mutations (K-Ras activation, N-Ras activation, and N-Ras ablation) to TNF-α and observed phenotypic and signaling changes in the intestinal epithelium. Hyperactivation of Mek1, an Erk kinase, was observed in the intestine of mice with K-Ras activation and, surprisingly, in N-Ras null mice. Nevertheless, these similar Mek1 outputs did not give rise to the same phenotype, as N-Ras null intestine was hypersensitive to TNF-α-induced intestinal cell death while K-Ras mutant intestine was not. A systems biology approach applied to sample the network state revealed that the signaling contexts presented by these two Ras isoform mutations were different. Consistent with our experimental data, N-Ras ablation induced a signaling network state that was mathematically predicted to be pro-death, while K-Ras activation did not. Further modeling by constrained Fuzzy Logic (cFL) revealed that N-Ras and K-Ras activate the signaling network with different downstream distributions and dynamics, with N-Ras effects being more transient and diverted more towards PI3K-Akt signaling and K-Ras effects being more sustained and broadly activating many pathways. Our study highlights the necessity to consider both environmental and genomic contexts of signaling pathway activation in dictating phenotypic responses, and demonstrates how modeling can provide insight into complex *in vivo* biological mechanisms, such as the complex interplay between K-Ras and N-Ras in their downstream effects

Introduction

Tumor necrosis factor alpha (TNF-α) is a pro-inflammatory cytokine whose function is pleiotropic and highly context-dependent. In the gastrointestinal tract, TNF-α drives chronic inflammatory conditions like Crohn's disease and ulcerative colitis. In this context, TNF-α is secreted into the extracellular milieu by immune and epithelial cells, where it engages

†This work was supported by grants from the National Institute of General Medical Sciences (R01-GM088827 to K.M.H., D.A.L.), the National Cancer Institute (U54-CA112967 to D.A.L.) and the Institute for Collaborative Biotechnologies from the U.S. Army Research Office (W911NF-09-D-000 to D.A.L). K.S.L. was a Robert Black Fellow of the Damon Runyon Cancer Research Foundation.

*Correspondence: khaigis@partners.org and lauffen@mit.edu.
‡These authors contributed equally.

TNF receptors 1 and 2 (TNFR1/2) for signaling. While TNFR1/2 are known to signal through two opposing pathways, the caspase-dependent apoptotic pathway and the NF-κB cell survival pathway, recent studies have revealed the context dependent functional pleiotropy of TNF-α. For example, TNF-α induces apoptosis in colorectal cancer cells and proliferation in glioblastoma cells.[1, 2] Similarly, we found that different regions of the same tissue can exhibit polar responses to TNF-α.[3] Given the contextual dependence of TNF-α function, one can envision the complex response of intact tissues to TNF-α *in vivo*. In an *in vivo* environment, cells are exposed to a variety of extrinsic and intrinsic perturbations that independently affect the signaling network and can consequently influence TNF-α function.

A useful strategy for studying complex biological phenomena, such as the pleiotropic activity of TNF-α, is to consider the behavior of a network state, rather than isolated pathways, using a systems biology approach. Using mathematical modeling to integrate information across a multitude of core pathways, we have shown previously that prediction of TNF-α-induced cell behaviors can be accurately depicted under a variety of different *in vivo* contexts.[3, 4] For example, we determined that the mitogen activated protein kinase (MAPK) signaling cascade is an important node that specifies the context for TNF-α-signaling, and consequently, TNF-α-dependent phenotypes.[3] Like TNF-α, the canonical Raf-Mek1-Erk signaling pathway can affect different biological processes depending on cellular context.[5–8] In the intestine, non-cell-autonomous growth factor activation of this pathway is important for epithelial repair during inflammation[9], probably through the regulation of the stem cell niche.[10] There is also evidence that the MAPK pathway functions to promote cell death triggered by pro-inflammatory death ligands (FasL, TRAIL, TNF-α).[11, 12] The MAPK cascade is downstream of Ras oncoproteins, a family of small GTPases that plays a significant role in colorectal carcinogenesis. Because chronic relapsing intestinal inflammation, a process driven by TNF-α, can drive colorectal cancer and *vice versa*, understanding how the inflammatory network interacts with Ras signaling to control phenotypic outcomes will shed light on both normal intestinal physiology and pathogenesis.

The Ras protein family consists of four highly homologous members: K-Ras4A, K-Ras4B, N-Ras, and H-Ras, all of which are thought to respond to the same upstream stimuli. Whereas mutations in H-Ras are not found in colorectal cancer, activating mutations in the other family members are common, with mutations in K-Ras and in N-Ras found in ~40% and ~3% of colorectal cancers, respectively.[13] This difference in mutation frequency suggests that the Ras isoforms are functionally distinct, which may be due to their different expression levels[14, 15], post-translational modifications in the hypervariable regions[16], and distinct subcellular localizations.[17, 18] Deciphering how these biochemical differences dictate the distinct function roles of the different Ras isoforms is an active area of research.

We recently studied the effects of Ras protein mutations on the *in vitro* response of colorectal cancer cells to TNF-α. Whereas activated K-Ras sensitized intestinal epithelial cells to TNF-α-induced cell death *in vitro*, activated N-Ras was protective.[19] To resolve the effect of altering different Ras isoforms on TNF-α signaling in a physiologically relevant context, we employed a systems biology approach to query and integrate the network signaling state of epithelial cells in response to TNF-α in the mouse intestinal epithelium under different Ras perturbations. The results here demonstrate the diversity of downstream signaling effects generated by the different Ras isoforms *in vivo*, which in turn distinctly modulate downstream TNF-α-induced cell death in the intestinal epithelium.

Results

The canonical signaling pathway downstream of Ras activation is the Raf-Mek-Erk MAPK cascade. In this pathway, GTP-loaded Ras proteins recruit Raf kinases to cell membranes to

be phosphorylated. Active Raf triggers phosphorylation and activation of Mek kinases, which subsequently phosphorylate Erk (Fig. 1A). Phosphorylated Erk can control a variety of cellular processes, including cell proliferation and cell death, through regulation of cytoplasmic targets or gene expression in the nucleus. Although oncogenic activation of this pathway in cancer is usually associated with proliferation, MAPK signaling is pro-death when intestinal epithelial cells are stimulated with TNF-α.[19] Hence, one might hypothesize that the function of the Raf-Mek-Erk pathway is context-dependent; that is, the phenotypic outcomes arising from pathway activation are controlled by the activation states of other pathways in the signaling network (Fig. 1A). The same can be said for TNF-α signaling. To investigate how extrinsic and intrinsic stimuli cooperate to control cellular behaviors, we have previously optimized methods to investigate *in vivo* network-level effects on TNF-α-induced cell death in the mouse intestinal epithelium. Briefly, we administered TNF-α intravenously to mice, and then isolated tissues from different locations of the intestine over a 4-hour time course. We have previously demonstrated that TNF-α induces apoptosis in the duodenum, but proliferation in the ileum, and that loss of the innate immune system in the gut potentiates apoptosis in the duodenum.[3, 4] Using our previous work establishing *in vivo* systems analysis approaches for gaining insights concerning molecular regulation of tissue pathophysiology, we first employed Partial Least-Squares Discriminant Analysis (PLSDA) to ascertain quantitative combinations of the key signaling node subsets most effectively accounting for differences in cell phenotypic responses across all the different conditions [3, 4]. PLSDA reduces the dimensionality of 'signal-response' relationships, enabling focus on the most important molecular governors. In our case, the PLSDA model focused signaling data from a 60-dimensional space into 2 latent variables ('quasi-eigenvectors' of signal-response space – the quantitative combinations of key signaling node subsets). The resulting model was able to capture network-level information related to different cell death-modifying conditions (Fig. 1B).[4] Latent variable (LV) 1 classified the signaling data with respect to the presence or absence of TNF-α-induced cell death (duodenal versus ileal tissues), while LV2 classified the signaling data by the magnitude of cell death (duodena of Rag1 null mice vs. WT mice). A major variable controlling the magnitude of apoptosis was a component of the MAPK signaling pathway, phosphorylated Mek1. Compared to WT control, phosphorylated Mek1 was significantly up-regulated at all points of the TNF-α time course in the duodenum of Rag1 null mice, where the epithelium was hypersensitive to TNF-α-induced apoptosis (Fig. 1C). In WT mice with MCP-1 ablation or exposure to IFN-γ, conditions that were not used to train the model but also sensitized the duodenal epithelium to TNF-α-induced cell death, phosphorylated Mek1 was also up-regulated by TNF-α compared to the respective controls (Supplementary Fig. 1A, B). Given the correlation between high MAPK signaling and high magnitude of TNF-α-induced cell death, we posit that this pathway impinges upon signaling downstream of TNFR to impact cellular behavior in response to TNF-α stimulation.

Since mutations in Ras family members can influence the activation state of the MAPK pathway, we hypothesized that perturbation of upstream Ras signals would indirectly alter TNF-α-dependent epithelial cell phenotypes. To test this hypothesis *in vivo*, we performed experiments on mice expressing activated K-Ras or N-Ras (*Villin-Cre/+ ; Kras*$^{LSL\text{-}G12D}$ or *Villin-Cre/+ ; Nras*$^{LSL\text{-}G12D}$) specifically in the intestinal epithelium.[20] We also generated animals that lack N-Ras (*Villin-Cre/+ ; Nras*$^{2lox/2lox}$) specifically in the intestinal epithelium.[21] These mice, along with those with the control *Villin-Cre* transgene only (referred to as WT control), were then subjected to TNF-α administration over a time course of 4 hours to observe the effects of Ras perturbation on TNF-α signaling.

Using phosphorylated Mek1 as a surrogate, we evaluated the ability of TNF-α to induce MAPK signaling under different situations of Ras perturbation. TNF-α was able to induce a moderate increase in Mek1 phosphorylation from baseline in the duodenal epithelium of WT

control animals (Fig. 1C).[3] Activated K-Ras increased Mek1 phosphorylation in un-stimulated duodenal tissues, while activated N-Ras did not have this ability, similar to what was previously observed in colonic tissues (Fig. 1C).[20] Interestingly, although K-Ras and downstream MAPK were already constitutively active in K-Ras mutant mice, TNF-α-stimulation further increased Mek1 phosphorylation that was sustained through 4 hours (Fig. 1C). TNF-α transiently and modestly increased Mek1 phosphorylation in the N-Ras activated background compared to WT control (Fig. 1C). Deletion of N-Ras slightly decreased basal Mek1 phosphorylation, but paradoxically up-regulated TNF-α-induced phospho-Mek1 in a sustained manner, however, the level of activation was lower than that of K-Ras mutant mice. Taken together, these initial observations indicate that altering upstream activities of different Ras isoforms can differentially perturb the downstream MAPK pathway, which may have important consequences on TNF-α-induced phenotypic outcomes in the intestinal epithelium.

The duodenal epithelium is prone to TNF-α-induced cell death, as marked by significant increases in caspase 3 cleavage. Because of the connection between TNF-α-induced apoptosis and the MAPK pathway, we evaluated the changes in apoptotic phenotype in the duodenal epithelium under different perturbations of upstream Ras oncoproteins. Under all conditions, basal apoptosis was unchanged (Fig. 2A). However, upon TNF-α-stimulation, distinct phenotypic changes were observed in the different Ras genotypes. Duodenal epithelium with activated N-Ras exhibited a modest increase in the number of apoptotic cells upon TNF-α-stimulation (Fig. 2A), with magnitude and kinetics of caspase 3 cleavage similar to WT control mice (Fig. 2B). This result was expected, given the modest effect of activated N-Ras on TNF-α-induced Mek1 phosphorylation. Surprisingly, activated K-Ras also had minimal effects on TNF-α-induced cell death in the intestinal epithelium compared to WT control, even though Mek1 was greatly perturbed (Fig. 2A,B). In the case where N-Ras was deleted to cause elevated TNF-α-induced Mek1 activation, the number of apoptotic cells in the duodenal epithelium was greatly elevated post-TNF-α (Fig. 2A). TNF-α induced cell death with a higher magnitude and at an earlier time point (1 hour) in N-Ras null mice compared to WT control (Fig. 2B). Apoptosis was not observed in the ileum under any conditions (data not shown). Although activation of K-Ras or loss of N-Ras potentiated TNF-α-induced stimulation of MAPK, only loss of N-Ras altered the cell death phenotype. We surmised that although MAPK is an important node for modulating TNF-α-induced cell death, it is not itself sufficient to control phenotypic outcomes. In other words, an alteration of the MAPK pathway must take place within the correct cellular context to specify its effect on phenotype. These results are consistent with a previous study on the context-dependence of another MAPK perturbation, that of Mek1 inhibition, on TNF-α-induced outcomes.[3]

Proliferation of the epithelium is thought to follow intestinal damage for the purpose of tissue repair. In fact, chronic cycles of damage and proliferation are hallmarks of inflammatory bowel diseases. TNF-α also had a proliferative effect on epithelial cells. In the duodenum of WT control mice, basal proliferation in the crypt region (as measured by the amount of phospho-histone H3 staining per crypt area) was initially high. Upon TNF-α-stimulation, proliferation arrested at 0.5 hours and then recovered after 2 hours (Supplementary Fig. 2A, C). In the ileum, proliferation did not decrease at the early time point, but nevertheless increased at the later time point (Supplementary Fig. 2C). Although the number of proliferating cells was higher in the intestinal epithelium with activated K-Ras, the tissue architecture (villus/crypt size) was larger overall, which resulted in a similar proliferation measure (proliferation per crypt area) as other conditions (Supplementary Fig. 2B). Different Ras perturbations affected TNF-α-induced cell death differently, but none of these conditions significantly affected proliferation in the duodenum or ileum (Supplementary Fig. 2C–F). These results are not consistent with the idea that proliferation is directly coupled to intestinal cell loss as a means to maintain barrier function of the

epithelium, and suggest that proliferation is controlled by precise signaling mechanisms after damage.

We hypothesized that phenotypic outcomes induced by TNF-α are not driven only by the MAPK pathway alone, but in synergy with the cellular context. To evaluate the contextual effects of Ras perturbations on the TNF-α signaling network, we used the Bio-Plex bead-based ELISA platform to sample to quantify a core set of signaling pathway time courses after TNF-α induction in Ras mutant mice. The activation of many of the central signaling pathways was clearly different when Ras mutant animals were exposed to TNF-α (Fig. 2C, Supplementary Fig. 3). Because establishing which combinations of these pathways (i.e., the signaling context) modulate phenotypic changes was difficult to do intuitively, hierarchical clustering was performed across signals and conditions (Supplementary Fig. 4). Taking all signaling time points into account, we observed that signals from consecutive time points clustered together (e.g. p-Akt 2h and 4h), demonstrating the similarity between these time points (Supplementary Fig. 4A). Furthermore, mice from each Ras condition generally clustered together (except for activated N-Ras and Villin-Cre control), demonstrating reproducibility within our *in vivo* experimental system (Supplementary Fig. 4A). We additionally clustered each signal by time course, which demonstrated that many of the proteins thought to be co-regulated (for example, Atf2 and Creb, Erk and Stat3S, Akt and Gsk3) do behave similarly following TNF-α stimulation (Supplementary Fig. 4B). Interestingly, this clustering exercise also showed that not all preconceived signaling connects hold true *in vivo*. For example, Mek1 and Erk1 exhibited divergent behaviors (Supplementary Fig. 4B). Finally, clustering on the average of all biological replicates (Supplementary Fig. 4C) revealed that the signaling profiles from activated K-Ras mice were the most different from the rest, followed by N-Ras null mice. N-Ras activated mice were the closest to controls.

To delineate how the Ras signaling context is related to the TNF-α-induced cell death phenotype, we applied the signaling datasets obtained from the different Ras perturbations (as independent variable X) to the PLSDA model generated using other conditions of TNF-α-induced cell death (as dependent variable Y=f(X)) (Fig. 3A). The output of the PLSDA model consisted of 3 classes: (1) no apoptosis class, (2) low magnitude apoptosis class, and (3) high magnitude apoptosis class. Duodenal tissues from WT control and activated N-Ras mice had signaling data that classified into the low magnitude apoptosis class, consistent with their TNF-α-induced cell death phenotypes (Fig. 3A, Supplementary Fig. 5A). Similarly, signaling data from tissues with N-Ras deletion classified into the high magnitude class (Fig. 3A, Supplementary Fig. 5B). Activated K-Ras tissues also had high MAPK activities, similar to N-Ras null mice, but, surprisingly, did not classify into the high magnitude class. Instead, the signaling data from these tissues translocated towards the no apoptosis class, consistent with the lower magnitude of TNF-α-induced cell death these tissues exhibited (Fig. 3A, Supplementary Fig. 5C). These results demonstrated that it is the signaling context created by Ras perturbations, instead of single pathway effects, that modulates how TNF-α signals to induce apoptotic cell death.

Since the K-Ras mutant context appeared to be an outlier with respect to the relationship between TNF-α-induced signaling and TNF-α-induced cell death, we sought to understand this relationship in greater detail. We explored the loadings from the PLSDA model to determine the important signals for phenotypic classification. Signals that consistently correlated with either latent variable over all time points included p-Rsk, p-p38, p-Mek1, p-IκBα, p-c-Jun, p-Atf2, and p-Akt (Fig. 3B). Using these identified signals, we performed a trajectory analysis on the two conditions where MAPK signaling was altered: activated K-Ras and N-Ras null. Replacing all the important signals from these two Ras conditions with the same signals from WT controls placed all data points (representing each condition) into

the low magnitude class, serving as the starting point of the analysis. We then moved the data points in signaling space by adding back signals from each condition in a stepwise fashion (Fig. 3C, D). Because each move in the signaling space is a translation in vector space, the order by which the moves take place is not important. In N-Ras deleted tissues, elevated p-Rsk, p-IκBα, p-Akt, and p-Mek1 together shifted the signaling data point from the low magnitude class to the high magnitude class (Fig. 3C). In K-Ras activated tissues, although high p-Mek1 also shifted the signaling data point upwards towards the high magnitude class, the other 3 signals did not have a large effect. In addition, p-c-Jun and p-Atf2 shifted the data point towards the no apoptosis class (Fig. 3D). N-Ras deletion creates a context by which TNF-α activates several synergistic pathways along with MAPK signaling to drive a pro-death phenotype. In K-Ras activated tissues, the pro-death effect of TNF-α-induced MAPK signaling is counteracted by other signals, namely p-c-Jun and p-Atf2.

To elucidate more mechanistic insight concerning differential Ras isoform contributions to the TNF-α response *in vivo*, we trained logic models to the signaling data at 30 minutes from all conditions using the constrained Fuzzy Logic (cFL) approach, using cross-validation tests to ensure against over-fitting.[22] We treated both activating Ras conditions as stimuli, and N-Ras ablation as an inhibitor of N-Ras activity. Cell Net Optimizer was then used to train a customized prior knowledge network to the signaling datasets (Fig. 1A, Supplementary Fig. 6). This exercise resulted in an ensemble of logic models with a reasonable fit to the data, with an average mean squared error (MSE) of 0.0519 (Supplementary Fig. 7A, B). The overall topology of the data-driven model represented how the TNF-α signal is routed through different pathways into measured phospho-protein nodes as constrained by given experimental data. Refinement of the model by heuristically altering the prior knowledge network and enhancing the parsimony of the simulations (i.e., by excluding expansion of “and” gates in model training) further improved the model fits (average MSE = 0.0413, p-value = 9.3788e-12) (Supplementary Fig. 8A, B).

The cFL does not consider feedback loops in order to facilitate the convergence of the simulations. Hence, it may miss the possibility of autocrine signaling in the system, for example, TNF-α-induced secretion of extracellular factors that further activate the signaling network [23]. We manually added edges in the prior knowledge network from an artificial growth factor node (assumed to be secreted in response to TNF-α) that signals through N-Ras and to K-Ras to depict TNF-α-induced growth factor signaling (Fig. 4A). The new family of models showed an improved fit (average MSE = 0.0372, p-value = 2.1878e-105, cross validation MSE = 0.0937) (Fig. 4B), and highlighted interesting connections by which different Ras isoforms differentially affect the signaling network. K-Ras and N-Ras were predicted to regulate cell survival, partially consistent with experimental results, but through different pathways. N-Ras was predicted to be an important upstream regulator of PI3K signaling, while K-Ras was predicted to activate several downstream signals, primarily the canonical MAPK pathway (Fig. 4A). The different parts of the signaling network that N-Ras and K-Ras exert control over may explain differences in phenotypic outcomes as a response to external stimulation, despite similar behaviors in other key signals.

The same approach, when applied to the signaling data at 60 minutes, yielded a different picture of the TNF-α-induced network activation (Fig. 4C, D). While K-Ras still maintained connections to MAPK and Map3k1 signaling, the connections between N-Ras and any other nodes were significantly diminished (Fig. 4C). This result suggested that N-Ras is only important in modulating early signals in response to TNF-α, consistent with the transient nature of N-Ras effects on TNF-α signaling *in vivo*. In contrast, K-Ras can affect the signaling network in a sustained manner, again consistent with experimental data.

Edges leading to IκBα were interesting in that they experienced differential regulation temporally by Ras. IκBα was preferentially regulated by N-Ras at the early time point, when N-Ras is most active. At the later time point, IκB-α signal regulation was replaced by K-Ras. This result suggested that K-Ras and N-Ras can functionally interact, and a balance between K-Ras and N-Ras activation is paramount for controlling the overall signaling network state. Indeed, when N-Ras was ablated, signals were modulated in a sustained manner, consistent with K-Ras dominated signaling. Although most signaling edges from K-Ras remained similar across the time-points, some important differences were noted. In particular, edges leading to Jnk (and downstream c-Jun and Atf2) originated from Ras proteins at the 30-minute time point, but directly from TNF-α at the later time-point (Supplementary Fig. 9). Temporal control of the signaling network may yet be another mechanism for K-Ras and N-Ras to differentially modulate phenotypic outcomes.

Discussion

In this study, we examined the role that context plays in TNF-α-induced cell death and proliferation in the intestinal epithelium by studying the effects of different Ras perturbations. Although the MAPK signaling pathway has previously been shown to positively correlate with cell death[4], our data suggest that this pathway requires additional contextual information to specify its function in the case of Ras mutations. For example, activation of K-Ras and loss of N-Ras both increased Mek1 phosphorylation, but only loss of N-Ras increased TNF-α-induced apoptosis. A survey of major core pathways in the intestine revealed that, in addition to the MAPK cascade, Ras perturbations had different effects on the network signaling state, i.e., the cellular context. When stimulated with TNF-α, intestinal epithelial cells without N-Ras responded by up-regulating a set of four pathways (p-Rsk, p-IκBα, p-Akt, and p-Mek1) that together were pro-death, as predicted by a mathematical model constructed with previous data. In contrast, TNF-α did not stimulate this set of pathways in K-Ras cells, and, in addition, had a muted p-c-Jun/p-Atf2 response. When these effects were combined with mathematical modeling, TNF-α-induced cell death was predicted to be reduced, consistent with experimental results. Furthermore, TNF-α-induced activation of N-Ras and K-Ras was predicted to differentially control different aspects of the signaling network, with N-Ras regulating PI3K and K-Ras regulating MAPK pathways. These predictions are consistent with published studies along two complementary avenues. For example, in cancers expressing mutant forms of Ras, activating mutations in the PI3K signaling pathway are less frequent in the context of N-Ras mutation and more common in the context of K-Ras mutation [24]. Moreover, N-Ras mutant tumors, in contrast to K-Ras mutant tumors, show clearly disparate responses in particular to PI3K inhibitors versus MEK inhibitors [25]. Thus, the network logic differences elucidated in our modeling study here are buttressed by literature reports in the genetic and therapeutic realms.

N-Ras and K-Ras also exerted different temporal effects on the signaling network, with N-Ras effects being transient and K-Ras effects being sustained, with their interaction having profound effects on downstream network activation and phenotype. These results speak to the importance of cellular context in dictating phenotypic outcomes in tissue responses. That is, a single pathway may not be sufficient to dictate cellular behavior; rather, it is how that pathway acts in conjunction with the whole signaling network that is important.

Recent studies have shed light on the molecular mechanisms that govern the different functions of K-Ras versus N-Ras. Because of different post-translational modifications in their hypervariable regions, Ras isoforms can occupy distinct locations inside the cell. Although all Ras isoforms can be farnesylated, the predominant form of K-Ras (K-Ras4B) has a polybasic region that targets it to the plasma membrane.[26] In contrast, N-Ras is palmitoylated in a dynamic fashion and is cycled between the plasma membrane and the

Golgi apparatus[27], where it has the potential to engage in different signaling pathways.[17] This molecular difference may contribute to the observed transience of N-Ras signal network activation compared to the sustained signaling of K-Ras, as was shown by logic modeling and observed experimentally. While on the cell surface, alternative postranslational modifications can further affect Ras association with membrane microdomains. K-Ras resides in cholesterol-independent microdomains and forms nanoclusters with galectin-3 when loaded with GTP.[28, 29] Meanwhile, palmitoylated N-Ras is associated with cholesterol-rich microdomains to trigger the formation of an alternative signaling complex, namely Stat3 and c-Raf, to promote cell survival in response to apoptotic stimuli.[30] Differential localization of Ras isoforms can induce the formation of different effector complexes, and consequently affect downstream cellular behaviors.

Although these studies have emphasized the molecular differences between K-Ras and N-Ras, these two proteins still share very high homology and many of the same effectors. As such, there can be significant competition between the two Ras proteins for downstream proteins, resulting in functional interaction between pathways. In a model called 'competitive equilibrium', it has been suggested that competition for, and saturation of, downstream effectors can be a mechanism of cell death control in K-Ras mutant versus isogenic K-Ras WT isogenic cancer cell lines.[31] In that model, activated K-Ras is a dominant competitor for N-Ras effectors for anti-apoptotic signaling, causing insensitivity of this pathway even though N-Ras is hyperactivated. Similarly, in another model called the 'galectin switch', galectin-3 clustering activates K-Ras at the expense of N-Ras signaling, causing a shift of signaling network activation away from Akt towards the MAPK pathway.[29] K-Ras activation can downregulate N-Ras signaling by a Mek1-dependent negative feedback loop.[32] In our system, ablating N-Ras can paradoxically activate MAPK signaling, and convert the transient signaling network dynamics to sustained signaling, suggesting a shift towards K-Ras signaling. However, eliminating N-Ras may also have resulted in the removal of N-Ras-dependent cell survival signaling, resulting finally in a pro-death context. Hence, the balance between N-Ras and K-Ras, and the competition for downstream effectors, may alter the signaling network in non-intuitive and multivariate ways. Our study clearly emphasizes the strength of combining both computational modeling and quantitative multi-variate experimentation to gain integrative network-level understanding of complex biological phenomena that cannot be easily obtained by traditional univariate reasoning.

Methods

Animals

Experimental animals used in this study were 8-week-old male mice. *Villin-Cre* [33], *Kras*$^{LSL\text{-}G12D/+}$ [34], *Nras*$^{LSL\text{-}G12D/+}$ [20], and *Nras*$^{2lox2/2lox2}$ [21] mice have been described previously. Animals carrying the *Kras*$^{LSL\text{-}G12D/+}$, *Nras*$^{LSL\text{-}G12D/+}$, and *Nras*$^{2lox2/2lox2}$ alleles were crossed with animals carrying the *Villin-Cre* transgene to either express constitutively active K-Ras or N-Ras from their endogenous loci, or to delete N-Ras specifically in the intestinal epithelium. *Villin-Cre* drives recombination uniformly in epithelial cells throughout the entire intestinal tract starting at the post-implantation stage during embryogenesis. Mice with activated K-Ras (*Kras*$^{LSL\text{-}G12D/+}$; *Villin-Cre/+*), activated N-Ras (*Nras*$^{LSL\text{-}G12D/+}$; *Villin-Cre/+*), N-Ras deletion (*Nras*$^{2lox2/2lox2}$; *Villin-Cre/+*), and control *Villin-Cre* transgene only (*Villin-Cre/+*, also referred to as WT control in the text) were then subjected to TNF-α administration over a time course of 4 hours to observe the effects of Ras perturbation on TNF-α signaling. All animal work performed in this study was undertaken according to approved protocols and animal welfare regulations as put forth

by the Subcommittee on Research Animal Care (SRAC) at the Massachusetts General Hospital.

Signaling data were derived from 15 mice for each condition/genotype - 5 time points and 3 mice at each time point. No littermates were used for biological replicates. All models were constructed with time course data from all 15 animals of a given genotype.

TNF-α administration and sample collection

Animals were anesthetized with Avertin (tribromoethanol, 250 mg/kg in PBS, Sigma-Aldrich), and then administered 5 μg of recombinant mouse TNF-α (Abazyme) in phosphate buffered saline (PBS, 50 μl total volume) by retro-orbital injection. Animals were then sacrificed at different time points post TNF-α treatment to compose a time course of collected tissues. Control animals were anesthetized, injected with PBS (50 μl) by retro-orbital injection, and then sacrificed 2 hours later. Sacrificed animals were dissected and their small intestines were removed. The small intestine was flushed with PBS supplemented with protease inhibitor, and then homogenized immediately in Bio-Plex lysis buffer (Bio-Rad) or fixed with formalin for immunohistochemistry. Duodenal samples were obtained from the 1 cm of small intestine immediately adjacent to the stomach. Ileal samples were obtained from the 3 cm of small intestine immediately adjacent to the cecum.

Bio-Plex signaling analysis

Quantitative measurements of protein phosphorylation were collected from lysed tissue samples using Bio-Plex (Bio-Rad), a multiplexed, bead-based system for analyzing total and phospho-protein levels in suspension. The following signals were measured: phosphorylated inhibitor of nuclear factor B alpha (p-IκBα, Ser32 and Ser36), phosphorylated c-Jun N-terminal kinase (p-Jnk, Thr183 and Tyr185), p-Mek1 (Ser217 and Ser221), p-Erk1 (Thr202 and Tyr204) and p-Erk2 (Thr185 and Tyr187), p-Rsk (Thr359 and Ser363), p-p38 (Thr180 and Tyr182), p-c-Jun (Ser63), p-Atf2 (Thr71), p-Akt (Ser473), p-S6 (Ser235 and Ser236), phosphorylated signal transducer and activator of transduction 3 (p-Stat3, Ser727), p-Stat3 (Tyr705), phosphorylated Glycogen synthase kinase 3 (p-Gsk3α/β, Ser21, and Ser9), and phosphorylated cAMP response element-binding protein (p-Creb, Ser133). Tissue lysates were quantified via BCA (bicinchoninic acid, Pierce) and equal amounts of protein from each sample were used for the Bio-Plex assays: 4 μg of protein was used for assays of p-Jnk, p-Akt, p-Stat3 (Tyr705), and p-Atf2, whereas 1.5 μg of proteins was used for the rest of the assays. These protein amounts were determined experimentally to be within the linear ranges of activity of these assays on small intestinal tissue samples before this analysis. Each Bio-Plex measurement was normalized to the corresponding measurements from a control TNF-α time course (WT mice) on the same plate.

Phenotypic analysis

Apoptosis was measured by performing quantitative Western blotting (Licor) for the amount of cleaved caspase 3 (CC3, Cell Signaling) in the same tissue lysates that were used for Bio-Plex signaling analysis. Immunohistochemistry for cleaved caspase 3 (Cell Signaling) and phosphorylated histone H3 (Cell Signaling) was performed by standard methodology. Proliferation was quantified using ImageJ. Briefly, phospho-histone H3 positive and negative regions in the crypt epithelium were segmented by their intensities. The areas of all phospho-histone H3 positive regions were then divided by the total area of the crypt epithelium to obtain a fractional proliferative measure.

Statistical Testing

Pairwise comparisons between time course datasets generated from different experimental conditions (for example, N-Ras null versus Control) were performed using 2-way analysis of variance (ANOVA) (Tables S1, S2). These analyses were then followed by Bonferroni post tests to compare data at individual time points (Table S3).

PLS Modeling

PLS discriminant analysis was performed with MATLAB PLS Toolbox 6.5 (Eigenvector) as using data described previously.[4] TNF-α time course datasets from animals with Ras perturbations were applied to the model as validation datasets. For trajectory analysis, the average of three biological replicates was used for each perturbation condition. Major loadings (signal contribution to direction of an LV) were selected by their uni-directional contribution over the whole time course. For each perturbation dataset, the identified signals were replaced with those from the WT control, placing all datasets initially in the low magnitude class. Each signal was then returned to the dataset, and the resulting score displacements were calculated and plotted onto LV space. A trajectory was mapped out for each Ras perturbation from the composite of all score displacements of that condition.

Training of models to data with constrained fuzzy logic

Data were normalized between zero and one as follows: signaling data at all time points were normalized relative to their value under the same conditions at time zero. Relative data were further normalized to the maximum value of each signal observed over all time points and conditions. The value of Mek1 under the Mek1 inhibitor condition was removed before normalization. Models were then trained to data as described previously[22], using the Cell Net Optimizer package in MATLAB. A prior knowledge network was developed from databases and literature, compressed and expanded as described in ref. [35] to include either all two input “and-not” gates, or to include only “or” gates. This model was then trained to data using a genetic algorithm designed to optimize normalized hill transfer functions of edge (instead of discrete Boolean values), specifying both the existence of each edge as well as parameters. As the genetic algorithm is stochastic, many simulations were run to produce a family of models with similar fits as determined by mean squared error. Models were further refined to remove edges that do not adversely affect the fit, and an optimally refined model was selected for further analysis. Ensemble topologies and fits from the family of refined models were generated using scripts available in Cell Net Optimizer. A ten-fold random cross validation was done on our best performing 30-minute model by subletting the data into 10 groups, and training the model to the remaining data for each subset. We tested significance of resulting MSE distributions from our different models using the Wilcoxon Rank Sum Test.

Supplementary Material

Refer to Web version on PubMed Central for supplementary material.

Abbreviations

TNF-α	tumor necrosis factor alpha
MAPK	mitogen activated protein kinase
Erk	extracellular signal regulated kinase
cFL	constrained fuzzy logic

WT	wild-type
PLSDA	partial least squares regression analysis
MSE	mean squared error

References

1. Janes KA, Albeck JG, Gaudet S, Sorger PK, Lauffenburger DA, Yaffe MB. Science. 2005; 310:1646–1653. [PubMed: 16339439]
2. Radeff-Huang J, Seasholtz TM, Chang JW, Smith JM, Walsh CT, Brown JH. J Biol Chem. 2007; 282:863–870. [PubMed: 17114809]
3. Lau KS, Juchheim AM, Cavaliere KR, Philips SR, Lauffenburger DA, Haigis KM. Sci Signal. 2011; 4:ra16. [PubMed: 21427409]
4. Lau KS, Cortez-Retamozo V, Philips SR, Pittet MJ, Lauffenburger DA, Haigis KM. PLoS Biol. 2012; 10:e1001393. [PubMed: 23055830]
5. Michaloglou C, Vredeveld LC, Soengas MS, Denoyelle C, Kuilman T, van der Horst CM, Majoor DM, Shay JW, Mooi WJ, Peeper DS. Nature. 2005; 436:720–724. [PubMed: 16079850]
6. Lin AW, Barradas M, Stone JC, van Aelst L, Serrano M, Lowe SW. Genes Dev. 1998; 12:3008–3019. [PubMed: 9765203]
7. Santos SD, Verveer PJ, Bastiaens PI. Nat Cell Biol. 2007; 9:324–330. [PubMed: 17310240]
8. Overmeyer JH, Maltese WA. Front Biosci. 2011; 16:1693–1713.
9. Dube PE, Yan F, Punit S, Girish N, McElroy SJ, Washington MK, Polk DB. J Clin Invest. 2012; 122:2780–2792. [PubMed: 22772467]
10. Sato T, van Es JH, Snippert HJ, Stange DE, Vries RG, van den Born M, Barker N, Shroyer NF, van de Wetering M, Clevers H. Nature. 2011; 469:415–418. [PubMed: 21113151]
11. Cagnol S, Van Obberghen-Schilling E, Chambard JC. Apoptosis. 2006; 11:337–346. [PubMed: 16538383]
12. Lim SC, Duong HQ, Parajuli KR, Han SI. Oncol Rep. 2012; 28:1429–1434. [PubMed: 22824956]
13. Lau KS, Haigis KM. Mol Cells. 2009; 28:315–320. [PubMed: 19812895]
14. Leon J, Guerrero I, Pellicer A. Mol Cell Biol. 1987; 7:1535–1540. [PubMed: 3600635]
15. Omerovic J, Hammond DE, Clague MJ, Prior IA. Oncogene. 2008; 27:2754–2762. [PubMed: 17998936]
16. Ahearn IM, Haigis K, Bar-Sagi D, Philips MR. Nat Rev Mol Cell Biol. 2012; 13:39–51. [PubMed: 22189424]
17. Chiu VK, Bivona T, Hach A, Sajous JB, Silletti J, Wiener H, Johnson RL 2nd, Cox AD, Philips MR. Nat Cell Biol. 2002; 4:343–350. [PubMed: 11988737]
18. Plowman SJ, Hancock JF. Biochim Biophys Acta. 2005; 1746:274–283. [PubMed: 16039730]
19. Kreeger PK, Mandhana R, Alford SK, Haigis KM, Lauffenburger DA. Cancer Res. 2009; 69:8191–8199. [PubMed: 19789336]
20. Haigis KM, Kendall KR, Wang Y, Cheung A, Haigis MC, Glickman JN, Niwa-Kawakita M, Sweet-Cordero A, Sebolt-Leopold J, Shannon KM, Settleman J, Giovannini M, Jacks T. Nat Genet. 2008; 40:600–608. [PubMed: 18372904]
21. Xu J, Haigis KM, Firestone AJ, McNerney ME, Li Q, Davis E, Chen SC, Nakitandwe J, Downing J, Jacks T, Le Beau MM, Shannon K. Cancer Discov. 2013 In press.
22. Morris MK, Saez-Rodriguez J, Clarke DC, Sorger PK, Lauffenburger DA. PLoS Comput Biol. 2011; 7:e1001099. [PubMed: 21408212]
23. Janes KA, Gaudet S, Albeck JG, Nielsen UB, Lauffenburger DA, Sorger PK. Cell. 2006; 124:1225–1239. [PubMed: 16564013]
24. Janku F, Lee JJ, Tsimberidou AM, Hong DS, Naing A, Falchook GS, Fu S, Luthra R, Garrido-Laguna I, Kurzrock R. PLoS ONE. 2011; 6:e22769. [PubMed: 21829508]

25. Migliardi G, Sassi F, Torti D, Galimi F, Zanella ER, Buscarino M, Ribero D, Muratore A, Massucco P, Pisacane A, Risio M, Capussotti L, Marsoni S, Di Nicolantonio F, Bardelli A, Comoglio PM, Trusolino L, Bertotti A. Clin Cancer Res. 2012; 18:2515–2525. [PubMed: 22392911]
26. Hancock JF, Paterson H, Marshall CJ. Cell. 1990; 63:133–139. [PubMed: 2208277]
27. Goodwin JS, Drake KR, Rogers C, Wright L, Lippincott-Schwartz J, Philips MR, Kenworthy AK. J Cell Biol. 2005; 170:261–272. [PubMed: 16027222]
28. Prior IA, Muncke C, Parton RG, Hancock JF. J Cell Biol. 2003; 160:165–170. [PubMed: 12527752]
29. Shalom-Feuerstein R, Cooks T, Raz A, Kloog Y. Cancer Res. 2005; 65:7292–7300. [PubMed: 16103080]
30. Wang Y, Velho S, Vakiani E, Peng S, Bass AJ, Chu GC, Gierut J, Bugni JM, Der CJ, Philips M, Solit DB, Haigis KM. Cancer Discov. 2013; 3:294–307. [PubMed: 23274911]
31. Keller JW, Franklin JL, Graves-Deal R, Friedman DB, Whitwell CW, Coffey RJ. J Cell Physiol. 2007; 210:740–749. [PubMed: 17133351]
32. Vartanian S, Bentley C, Brauer MJ, Li L, Shirasawa S, Sasazuki T, Kim JS, Haverty P, Stawiski E, Modrusan Z, Waldman T, Stokoe D. J Biol Chem. 2013; 288:2403–2413. [PubMed: 23188824]
33. el Marjou F, Janssen KP, Chang BH, Li M, Hindie V, Chan L, Louvard D, Chambon P, Metzger D, Robine S. Genesis. 2004; 39:186–193. [PubMed: 15282745]
34. Tuveson DA, Shaw AT, Willis NA, Silver DP, Jackson EL, Chang S, Mercer KL, Grochow R, Hock H, Crowley D, Hingorani SR, Zaks T, King C, Jacobetz MA, Wang L, Bronson RT, Orkin SH, DePinho RA, Jacks T. Cancer Cell. 2004; 5:375–387. [PubMed: 15093544]
35. Saez-Rodriguez J, Alexopoulos LG, Epperlein J, Samaga R, Lauffenburger DA, Klamt S, Sorger PK. Mol Syst Biol. 2009; 5:331. [PubMed: 19953085]

Insight, innovation, integration

Since cells in their physiological context are simultaneously exposed to multiple stimuli, they must integrate network-level information to arrive at a coherent response. As a result, activation of any given signaling pathway can have divergent effects on cellular behavior. We have employed an approach that integrates systems biology with mouse genetics to provide biological insight into the network signaling effects of K-Ras and N-Ras mutations and their relationships to phenotypic outcomes when intestinal epithelial cells are exposed to TNF-α. Our study provides a formal demonstration that activation of a singular canonical pathway is not predictive of phenotypic outcome in a complex physiological environment and that an in vivo systems biology approach evaluating contextual information induced by different conditions is required to predict and understand complex biological phenomena.

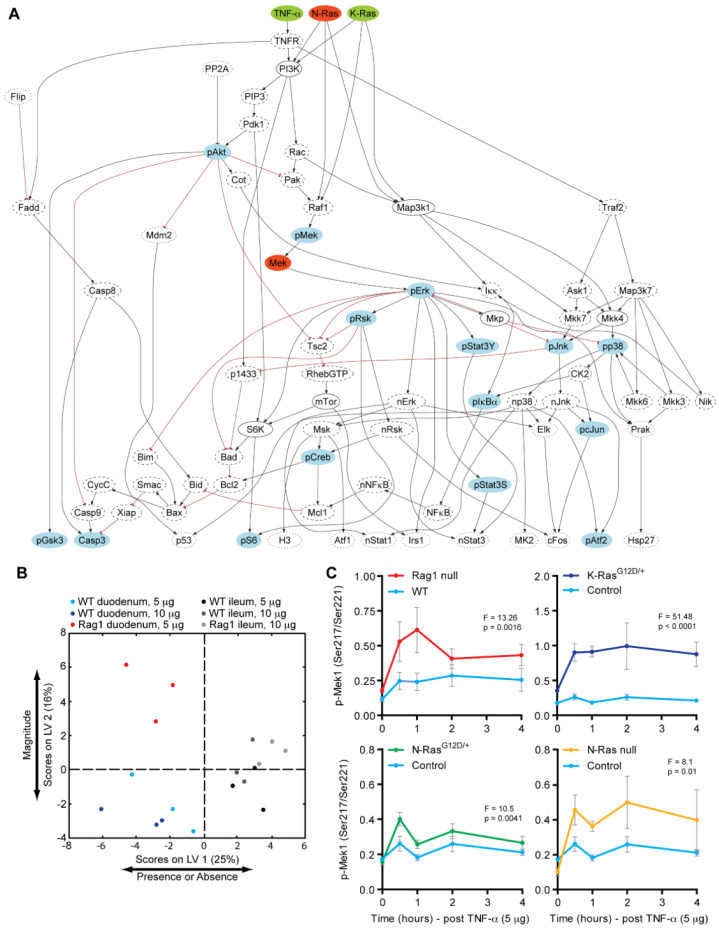

Fig. 1. TNF-α-induced MAPK signaling is differentially affected by Ras perturbations in the intestinal epithelium

(A) Prior knowledge network demonstrating TNF-α and Ras signaling pathways in the context of the rest of the network. Signals highlighted in green represent inputs into the signaling network in our experiments. Signals highlighted in red present inhibitors (the N-Ras null condition is modeled as an inhibitor). Signals highlighted in blue were measured via Bio-Plex. (B) A two-dimensional PLSDA model constructed using signaling time courses obtained from different cell death modifying experiments. Each data point represents scores generated by the model, composed of all signaling time courses of a particular condition, mapped onto latent variable space. The two orthogonal latent variable axes separate the scores by cell death phenotype: LV1 by the presence or absence of cell death and LV2 by the magnitude of cell death. The percentages on the axes represent the percent variance in the dataset captured by a particular LV. (C) Phosphorylated Mek1 time course measured as a surrogate for MAPK pathway activation by TNF-α. p-Mek1 is elevated in a sustained manner in conditions that display a high magnitude of TNF-α-induced cell death, for example, in the case of Rag1 knockout compared to WT mice. K-Ras activation (K-Ras^{G12D}) up-regulates p-Mek1 in a sustained manner as a function of TNF-α, whereas N-Ras activation (N-Ras^{G12D}) does so in a transient manner. N-Ras ablation (N-Ras null) up-regulates p-Mek1 in a sustained manner similar to K-Ras, but to a lesser degree. Error bars represent SEM for 3 animals. Statistical analysis was done by 2-ANOVA test (Supplementary Table 1).

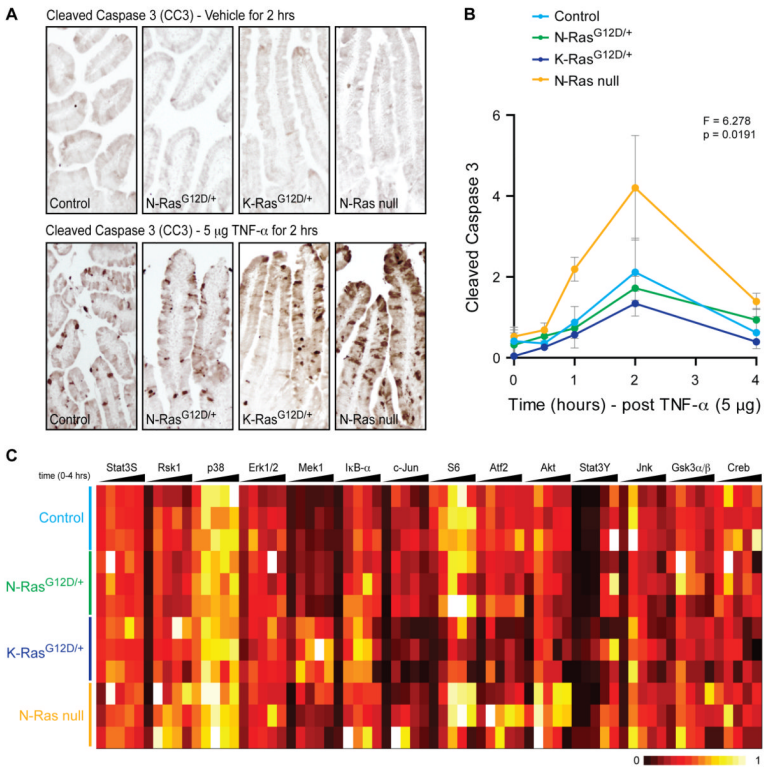

Fig. 2. Different Ras perturbations result in divergent phenotypic outcomes

(A) Cleaved caspase 3 immunohistochemistry of duodenal tissues from mice with different Ras perturbations treated with vehicle or TNF-α for 2 hours. TNF-α treated N-Ras null mice display an elevated intestinal cell death response compared to control. (B) Quantitative western blot analysis of cleaved caspase 3 in duodenal tissues of mice with different Ras perturbations, as a time course of TNF-α stimulation. N-Ras ablation results in higher magnitude of TNF-α induced caspase 3 cleavage occurring at an earlier time, while K-Ras^{G12D} slightly suppresses cell death. Error bars represent SEM for 3 animals. Statistical analysis was done by 2-ANOVA test (Supplementary Table 2). (C) Phosphorylation of protein nodes in central signaling pathways in duodenal tissue lysates by Bio-Plex. The heat map is organized such that the columns represent the phospho-signal time courses, while the rows represent different Ras perturbations. Each phospho-signal is arranged sequentially as a function of time (left to right, 0 to 4 h). The intensity of the heat map represents the average of technical duplicates of the median fluorescence intensity (normalized to the highest value of each signal) resulting from each assay. Data are compiled from three independent experiments for each perturbation.

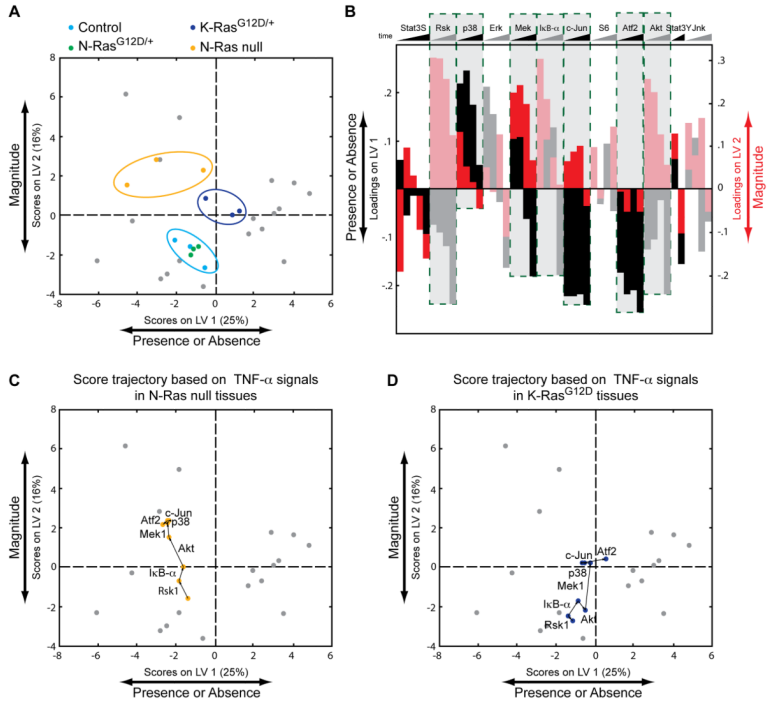

Fig. 3. PLSDA model predictions of phenotypic outcomes generated by the network context under different Ras perturbations

(A) TNF-α-induced phospho-signaling time courses from the duodena of mice with different Ras perturbations mapped onto the two dimensional LV space. Data from N-Ras^{G12D} and WT mice classify into the low magnitude class (lower left quadrant), while data from N-Ras null mice classifies into the high magnitude class (upper left quadrant). Data from mice with K-Ras^{G12D} displays mixed properties, and falls between the high magnitude class and the no apoptosis class. (B) Loadings on LV1 (black) and LV2 (red), the latent variable that correlates with the presence of cell death and the magnitude of cell death, respectively. The y-axis quantifies the positive or negative contribution of a particular signal to a latent variable. Loadings that contribute in a uni-directional manner over time are highlighted and considered to be important for that LV. (C) Trajectory analysis of scores from the N-Ras null signaling dataset. Signals that are important for the model (as identified in B) are replaced by those of the WT control, initially placing the data points into the low magnitude class. Signals from the original N-Ras null dataset are then returned one-by-one to recalculate the resulting displacement of scores in LV space. A pro-death signature characterized by 4 signals (identified previously) is responsible for the classification of the N-Ras null dataset into the high magnitude class. Data points represent the average of the signaling time course datasets between 3 independent experiments. (D) Trajectory analysis of scores from the K-Ras^{G12D} signaling dataset. Atf2 and c-Jun displaces the scores from the high magnitude class to the no apoptosis class.

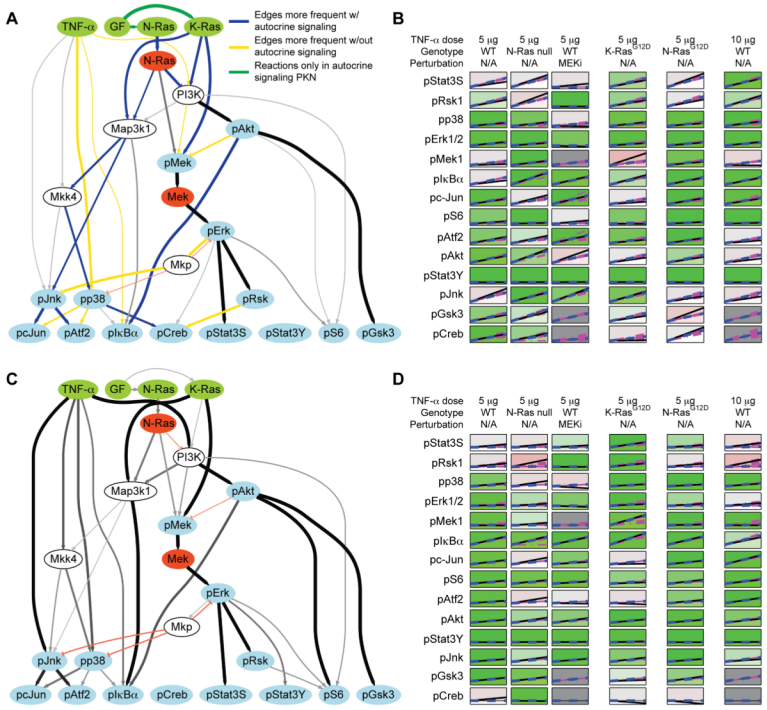

Fig. 4. Autocrine signaling changes topology and yields better fit of model to data at 30 minutes

(A) Ensemble topology of family of cFL models trained to data with autocrine signaling included in the prior knowledge network. The thickness of each edge represents the frequency at which it appears in the trained models. Edges are color-coded if they appear more or less (by 25%) frequently in the autocrine model than the model with no autocrine signaling. Nodes represent ligand stimulation or genetic activation (green), inhibitors or knockouts (red), measured phosphorylation sites (blue), or proteins that are not measured or perturbed, but cannot be compressed while maintaining logical consistency (white). (B) Fit of trained models in panel A to normalized data at 30 minutes. Normalized data (solid black lines), predicted values from individual models (pink dashed lines), and average of simulations from family of models (blue dashed lines) are plotted. The background color represents goodness of fit, with green being the least discrepant between simulation and data, red being the most, and gray background signifies that no data was available. (C) Ensemble topology of family of cFL models trained to data at 60 minutes. Edges are either activating (black) or inhibitory (red). (D) Fit of model to data at 60 minutes.